© 2021. Published by The Company of Biologists Ltd | Journal of Cell Science (2022) 135, jcs258322. doi:10.1242/jcs.258322

Intracellular flow cytometric lipid analysis – a multiparametric system to assess distinct lipid classes in live cells

Badwi B. Boumelhem[1], Chelsea Pilgrim[1], Vincent E. Zwicker[2], Jacek L. Kolanowski[2,*], Jia Hao Yeo[3], Katrina A. Jolliffe[2,4], Elizabeth J. New[2,4], Margot L. Day[1], Stephen J. Assinder[1,4] and Stuart T. Fraser[1,3,4,5,‡,§]

ABSTRACT

The lipid content of mammalian cells varies greatly between cell type. Current methods for analysing lipid components of cells are technically challenging and destructive. Here, we report a facile, inexpensive method to identify lipid content – intracellular flow cytometric lipid analysis (IFCLA). Distinct lipid classes can be distinguished by Nile Blue fluorescence, Nile Red fluorescence or violet autofluorescence. Nile Blue is fluorescent in the presence of unsaturated fatty acids with a carbon chain length greater than 16. *Cis*-configured fatty acids induce greater Nile Blue fluorescence than their *trans*-configured counterparts. In contrast, Nile Red exhibits greatest fluorescence in the presence of cholesterol, cholesteryl esters, some triglycerides and phospholipids. Multiparametric spanning-tree progression analysis for density-normalized events (SPADE) analysis of hepatic cellular lipid distribution, including vitamin A autofluorescence, is presented. This flow cytometric system allows for the rapid, inexpensive and non-destructive identification of lipid content, and highlights the differences in lipid biology between cell types by imaging and flow cytometry.

This article has an associated First Person interview with the first author of the paper.

KEY WORDS: Flow cytometry, Imaging, Lipids, Lipophilic dyes, Nile Blue, Nile Red

INTRODUCTION

Lipid metabolism is tightly regulated at the cellular, organ and whole-body levels (Frayn et al., 2006; Rui, 2011). Lipids are gained from diet or synthesised *de novo* from precursors. Critical lipid classes within mammalian cells include phospholipids, which form cell membranes, free fatty acids (FFA), cholesterol and triglycerides (TAGs), neutral lipids stored in droplets, and lipids involved in inter- or intra-cellular communications, such as steroids and phospholipids. Short chain fatty acids (SCFA), such as butyrate, regulate gene expression, whereas myristic acid and cholesterol modulate protein function (Astakhova et al., 2016; Hu et al., 2011).

Rates of obesity, diabetes and metabolic disorders are increasing globally. *In situ* or *in cellulo* detection of lipids by antibody staining is currently ineffective, as lipids are typically poor immunogens (Maekawa and Fairn, 2014). Liquid chromatography-mass spectrometry (LC/MS), although highly accurate in determining cellular lipid composition, is destructive (Cespedes et al., 2015; Kerwin et al., 1996; Murphy and Axelsen, 2011). There is clearly a need for methodologies that allow for the rapid detection of lipid classes in live mammalian cells.

Fluorescent dyes and probes can be useful for lipid detection in cells. Here, we have employed the lipophilic dyes Nile Red (NR) and Nile Blue (NB) to assess differences in neutral lipid and FFA composition across a range of tissues (Maekawa and Fairn, 2014). NR and NB are heterocyclic benzophenoxazines (Smith, 1911; Martinez and Henary, 2016). NB is positively charged and contains an iminium group whereas NR is neutral and contains a carbonyl group. NB detects bacterial polyhydroxybutyrate, although this staining may be due to NR contamination (Ostle and Holt, 1982). NR is a well-known fluorescent lipophilic stain and has been used to visualise lipid storage in a broad range of cell types from algae to humans (Greenspan et al., 1985; Rumin et al., 2015; McMillian et al., 2001; Dates et al., 2015). Previously, we demonstrated that NR could distinguish adipocyte heterogeneity at the single-cell level by flow cytometry (Boumelhem et al., 2017). Fluorescent probes can also be generated to sense specific lipids, including the probe P-IID, which we have recently reported as a sensor for extracellular phosphatidylserine (Zwicker et al., 2019).

Here, we report that NB fluorescence is induced by unsaturated FFA with at least 16 carbons. In contrast, NR fluoresces in the presence of cholesterol, cholesterol esters, some triglycerides and phospholipids. This identification of the lipid-specific NB and NR fluorescence, combined with the cell-permeable nature of both dyes has allowed us to utilise these dyes for live-cell imaging, histochemistry and flow cytometry, offering new perspectives on the heterogeneity and flux of lipids within mammalian cells. In combination with autofluorescence signals, these lipophilic probes can be used for intracellular flow cytometric lipid analysis (IFCLA).

RESULTS

NR and NB are cell-permeable fluorescent lipophilic dyes

The use of NB as a fluorescent stain of mammalian cells has not been extensively reported. Both NR and NB are fluorescent; NR can be excited at 488 nm and emits between 565 and 640 nm, whereas NB can be excited at 620 nm with emission between 630 and 700 nm. Cryosections of adult mouse tissues were fixed with 4% paraformaldehyde (PFA) in PBS, incubated with NB and NR, washed and imaged immediately. Confocal microscopy revealed that lipid droplets of brown adipose tissue (BAT) were stained by NR (Fig. 1Ai,ii). Laminar structures near the BAT vasculature were

[1]Discipline of Physiology, School of Medical Sciences, University of Sydney, Camperdown, NSW, 2050, Australia. [2]School of Chemistry, University of Sydney, Camperdown, NSW, 2050, Australia. [3]Discipline of Anatomy and Histology, School of Medical Sciences, University of Sydney, Camperdown, NSW, 2050, Australia. [4]University of Sydney Nano Institute, University of Sydney, Camperdown, NSW, 2006, Australia. [5]School of Biomedical Engineering, University of Camperdown, NSW, 2006, Australia.
*Present address: Institute of Bioorganic Chemistry, Polish Academy of Sciences, Poznan, 61-704, Poland. ‡Present address: School of Biomedical Engineering Link Building Faculty of Engineering and IT, The University of Sydney, Darlington, NSW 2006, Australia.

§Author for correspondence (stuart.fraser@sydney.edu.au)

S.J.A., 0000-0002-2206-2427; S.T.F., 0000-0003-3795-9461

Handling Editor: James Olzmann
Received 21 December 2020; Accepted 28 May 2021

Journal of Cell Science (2022) 135, jcs258322. doi:10.1242/jcs.258322

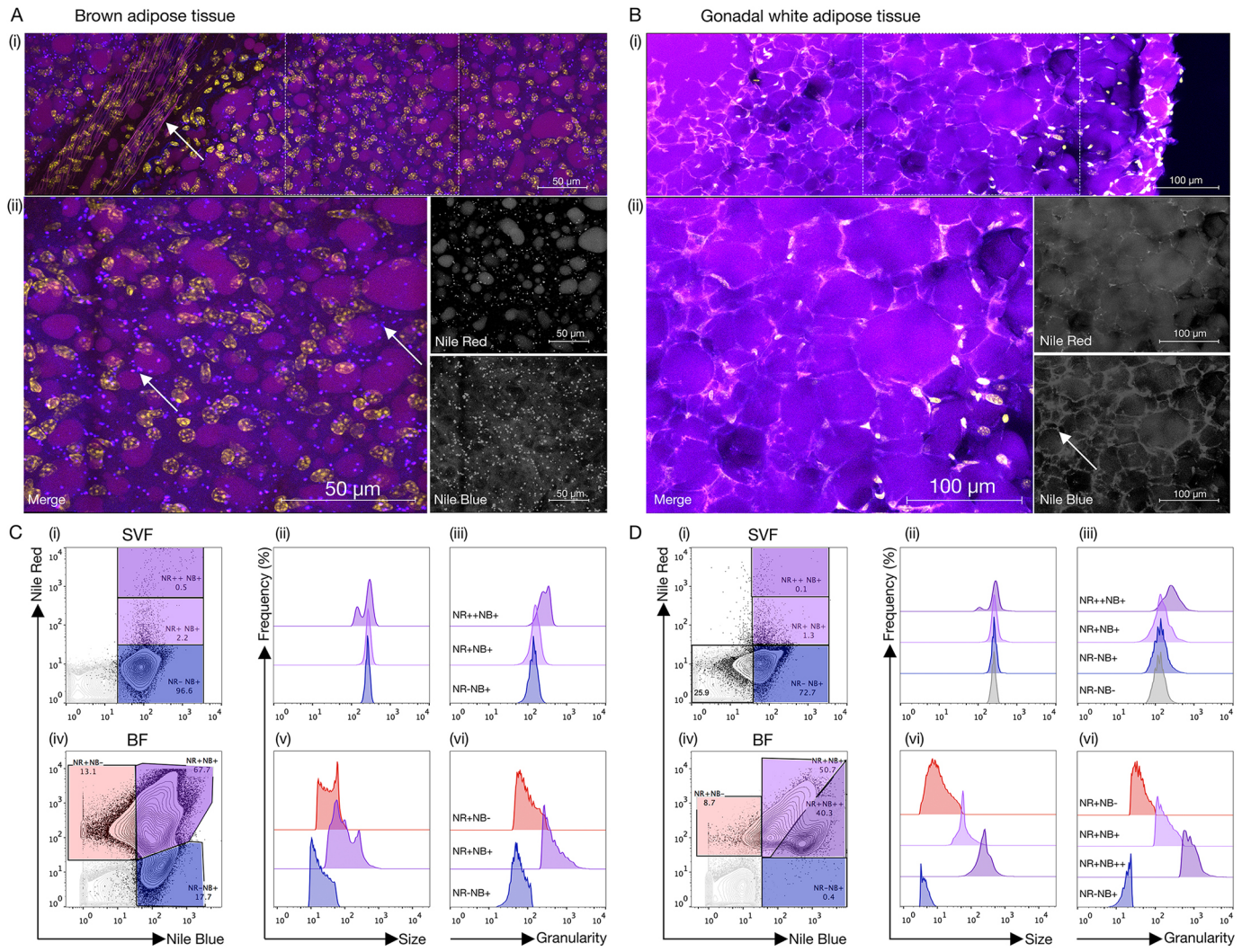

Fig. 1. Both NB and NR are cell-permeable, fluorescent lipophilic probes that fluoresce in mouse adipocytes. (A,B) Representative images of cryosections (20 µm) of mouse (Ai) brown and (Bi) gonadal white adipose tissue stained with NR (magenta), NB (blue) and DAPI (yellow). A *z*-stack of 20 µm was compiled for each sample. Images presented are a maximum intensity projection. Magnified regions (dotted box) of (Aii) brown and (Bii) gonadal white adipose tissue. White arrow in Ai indicates NR staining of laminar vessel-like structure. White arrows in Aii and Bii indicate NB staining of peroxisome-like structures. (C,D) Single-cell suspensions of (C) brown and (D) white adipose tissue were generated using the method previously published (Boumelhem et al., 2017). Cells of the stromal vascular fraction (SVF) (Ci–iii,Di–iii) and buoyant fraction (BF) (Civ–vi,Div-vi) were stained with NR and NB and fluorescent populations identified. Gates were applied according to fluorescence intensity. Grey shaded region, unstained cells ($NR^{-}NB^{-}$); red shaded region, NB negative ($NR^{+}NB^{-}$); pink-shaded region, NR-negative, NB-positive cells ($NR^{-}NB^{+}$); NR high, NB-positive cells ($NR^{++}NB^{+}$, magenta); NR- and NB-positive cells ($NR^{+}NB^{+}$). Numbers inside regions indicate percentage of cells in each area. All populations were then back-gated to analyse the forward (size) (Cii,Dii) and side (granularity) (Ciii,vi,Diii,vi) scatter profiles. For each cell preparation, at least 10^5 cells were analysed. Confocal microscopic images and flow cytometric data presented are representative and taken from at least three independent experiments.

also stained with NR (Fig. 1Ai, arrow). In contrast, NB fluorescence was largely observed in distinct punctate structures within the brown adipocytes (Fig. 1Aii, arrows). These punctate structures were ∼1 µm in diameter, stained with NB peripherally and NR centrally and resemble peroxisomes which are abundant in brown adipocytes (Fig. 1Aii) (Lodhi and Semenkovich, 2014; Ahlabo and Barnard, 1971; Park et al., 2019). Peroxisomes in brown adipocytes are involved in the metabolism of lipids through β- and α-oxidation of very long chain fatty acids and methyl-branched fatty acids (Park et al., 2019). NB diffusely stained the cytoplasm of gonadal white adipocytes with fluorescence that was most intense around the periphery of the cytoplasm (Fig. 1Bii). NR intensely stained the lipid droplets of adipocytes in white adipose tissue (WAT) (Fig. 1Bii). Compared to BAT, there were less peroxisome-like organelles stained with NB (Fig. 1Bii). This could be due to the characteristically large, triglyceride-rich lipid droplets, which constitute much of the cytoplasm in each white adipocyte. Thus, NR and NB can stain distinct intracellular features in brown adipocytes and, to a lesser degree, white adipocytes.

To assess the utility of NB for flow cytometry, single-cell suspensions of BAT and WAT were prepared with the buoyant fraction (BF), which contains adipocytes, and a stromal vascular fraction (SVF) (Boumelhem et al., 2017). Cells were incubated with NB and NR and flow cytometry performed. All SVF samples showed a similar pattern, with strong NB fluorescence and no or little NR fluorescence, demonstrating that NB is cell permeable and fluoresces in the presence of lipids within mammalian cells (Fig. 1Ci–iii,Di–iii). In contrast, the buoyant fraction in all tissues studied contained populations with NR and NB. BAT BF cells contained three populations, those that were NR-positive alone

Journal of Cell Science (2022) 135, jcs258322. doi:10.1242/jcs.258322

(NR^+), NB-positive alone (NB^+), or NR and NB double-positive cells (NR^+NB^+) (Fig. 1Civ–vi). NR^+NB^+ cells were larger and more granular compared to NR^+ or NB^+ cells, which may be indicative of the presence of peroxisomes inside BAT adipocytes (Fig. 1Civ–vi). More than 90% of buoyant white adipocyte cells were NB^+ (Fig. 1Div–vi). Gonadal WAT contained two populations with increasing NB intensity (Fig. 1Div–vi). Cells with the greatest NB fluorescence (NB^{++}) were the largest, most granular cells (Fig. 1Div–iv). These findings demonstrate that NB and NR can be combined to segregate distinct populations from adipose tissues. However, it is unclear which lipids the two dyes are detecting within these populations.

NB and NR lipid specificity

To determine why these structurally similar dyes show distinct lipid detection profiles within cells, spectrofluorimetric analysis of 70 different lipids in PBS was performed (Fig. 2; Table S1, Fig. S4). Neither NB nor NR was fluorescent in the presence of saturated fatty acids (Fig. 2A). NB fluoresced only in the presence of specific unsaturated fatty acids (Fig. 2A–C), the monounsaturated fatty acids palmitoleic and oleic acid, which are commonly found in mammalian cells, and linoleic acid, which is polyunsaturated and present in mammalian cells and is a precursor of arachidonic acid (Fig. 2A,B). Nervonic acid and erucic acid, which are elongation products of oleic acid, also induced high NB fluorescence.

Of the 22 unsaturated fatty acids assessed, NR fluoresced only in the presence of oleic acid (Fig. 2A). Other unsaturated fatty acids caused NR to fluoresce, but the emission maximum was red-shifted, with peak emission at 620 nm, beyond the range used to detect NR by flow cytometry or confocal microscopy (520–590 nm; Fig. S3, Fig. S4C). NR fluorescence was observed with cholesterol, cholesteryl esters and triglycerides (Fig. 2A). NR fluorescence was also observed in the presence of low- and high-density lipoproteins (Table S1). NR fluoresced in the presence of phosphatidylcholine (PC), phosphatidylserine (PS), platelet-activating factor (PAF) and the brain lipid glucosylceramide (Fig. 2A). PC and PS are components of the mammalian plasma membrane lipid bilayer; however, cell membrane staining has not been observed by histological staining. Neither NR nor NB showed any fluorescence response to the presence of steroids (Table S1). Lipids must contain 16 or more carbons to induce NR or NB fluorescence (Fig. 2A). Small and medium chain fatty acids failed to induce fluorescence in these liquid-based assays. The number and position of double bonds in the fatty acid chain did not significantly influence the observed intensity of NB fluorescence (Fig. 2B; Fig. S1). However, fatty acids with *trans*-configured double bonds, including palmitoleic, oleic, vaccenic, linoleic and eicosapentanoic acids displayed significantly lower fluorescence intensity than their *cis*-configured counterparts of equal carbon number (Fig. 2Ci,ii).

To determine whether the spectrofluorimetry data were pertinent to the behaviour of NR and NB in live cells, an array of lipids from multiple classes were added to cultures of mouse embryonic stem cells (ESCs) for 30 min prior to confocal imaging and flow cytometric analysis. NB fluorescence intensity increased in oleic acid-treated cells but not vehicle (DMSO)-treated cells, with diffuse and punctate cytosolic blue staining evident (Fig. 3Ai,ii,Bi,ii). When assessed by flow cytometry, only mouse ESCs treated with oleic and linoleic acids showed an increase in fluorescence intensity for NB (Fig. 3Bi,ii). No change in NB fluorescence intensity was observed for cells treated with saturated fatty acids, cholesterol, cholesterol esters, triglycerides and phospholipids, consistent with our finding above that NB fluorescence is restricted to unsaturated fatty acids (Fig. 2A, Fig. 3Bi). Therefore, NB exhibits specificity for *cis*-unsaturated FFAs.

An increase in NR fluorescence was detected in mouse ESCs treated with oleic acid only (P=0.02) (Fig. 3Bii). While NR fluoresces in the presence of cholesterol, cholesterol esters and triglycerides *in vitro* (Fig. 2A), mouse ESCs treated with those lipids did not lead to an increase in NR fluorescence (Fig. 3Bii). This could be due to the lack of uptake of these lipids in mouse ESCs due to the short incubation time or, alternatively, this could indicate that NR staining of lipid droplets in mouse ESCs is composed mostly of oleic acid (Fig. 3Bii).

Dynamic shifts in NR and NB fluorescence highlights changes in maternal–fetal lipid exchange throughout development

In rodents, the exchange of nutrients between mother and developing embryo takes place at the placental interface and the yolk sac (YS), a membrane that encapsulates the embryo/fetus. The YS is important for the transport of less-soluble nutrients such as lipids (Farese et al., 1996). NR fluorescence was localised to lipid droplets within the YS at all time points assayed (Fig. 4Ai–iii) with fluorescence greatest at embryonic day (E)10.5 of development and was diminished by E18.5 (Fig. 4Bi–iii). NB fluorescence was observed in the cytoplasm of YS epithelial cells (Fig. 4Bi–iii). Flow cytometry revealed two distinct populations of YS cells: one showing fluorescence of both dyes (NR^+NB^+) and another population which exhibited NB fluorescence alone (NR^-NB^+) (Fig. 4Bi–iii,Ci,ii). The frequency of NR^+NB^+ cells was greatest at E10.5 (Fig. 4Bi, Fig. 4Ci; Tables S2, S3). In contrast, NR^-NB^+ cell frequency was lowest in the earliest developmental stage assayed but significantly increased by E12.5, reaching maximum levels at E15.5 (Fig. 4Bi–iii; Tables S2, S3). At E14.5, there was a clear decline in NR^+NB^+ cells and an increase in NR^-NB^+ cells (Fig. 4Cii). Lipid content and transport in the mouse YS therefore dynamically changes throughout development and can be assessed by NB and NR fluorescence intensity.

NB and NR fluorescence discriminates distinct cell types in adult mouse organs

We next determined whether NR and NB can identify distinct populations in adult mouse tissues. In the adrenal gland, the cortex is composed of steroidogenic cells, whilst the medulla is rich with neuroendocrine chromaffin cells (Rosol et al., 2001). Intense NR staining was observed in lipid droplets across all cortical regions of the adrenal gland (Fig. 5Ai,ii). NB and NR staining were also observed in the cytoplasm in all cortical regions of the adrenal gland (Fig. 5Ai,ii). In contrast, the adrenal medulla showed few, if any, NR-positive lipid droplets and lower levels of NB fluorescence than the cortex (Fig. 5Ai,ii). Flow cytometric analyses revealed that the SVF fraction largely lacks NR fluorescence (Fig. 5Bi), suggesting these are predominantly medullary cells, whereas the buoyant fraction is dominated by NR and NB-stained cells, as seen in the cortex (Fig. 5Bii). NR and NB fluorescence could therefore be a useful method to isolate these distinct adrenal populations.

The testes contain seminiferous tubules with spermatozoa at different stages of development, supported by the Sertoli cells (Griswold, 1995; De la Torre et al., 1976; Hu et al., 2010). Within the interstitium between tubules, the Leydig cells synthesise androgens *de novo* from cholesterol (Hu et al., 2010). The seminiferous tubules exhibited a low NB signal indicating lower levels of free fatty acids (Fig. 5Ci,ii, yellow arrow). In contrast, cells distributed throughout the interstitium showed intense NR and NB fluorescence (Fig. 5Ci,ii, white arrows). The size, morphology and location all suggest that these are lipid-rich androgen-producing

Journal of Cell Science (2022) 135, jcs258322. doi:10.1242/jcs.258322

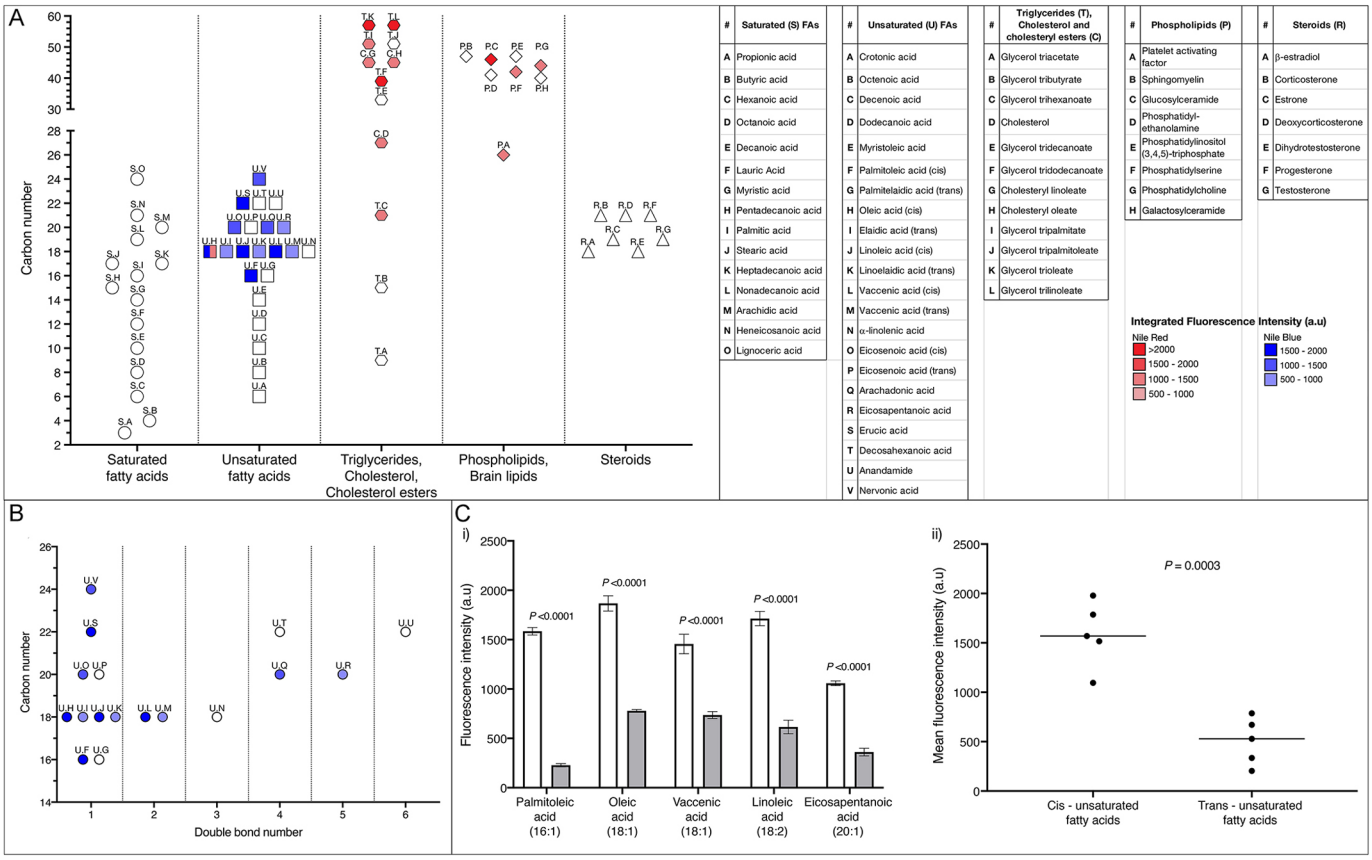

Fig. 2. Specificity of NB and NR fluorescence in the presence of different lipid classes. (A) Spectrofluorimetric analyses of saturated (S) and unsaturated (U) fatty acids. Triglycerides (T), cholesterol (C) and cholesterol esters (E); phospholipids (P) and brain (B) lipids and steroids (R) were performed in the presence of NR and NB in PBS. NR was excited at 488 nm while NB was excited at 620 nm. Emission was collected from 500 to 675 nm for NR and 640 to 800 nm for NB. Integrated fluorescence intensity (a.u.; arbitrary units) presented as different shades of red (NR) or blue (NB). (B) Comparisons between double bond number and carbon number of unsaturated fatty acids in the presence of NB. (Ci,ii) Comparisons between *cis* (white bars) and *trans* (shaded bars) unsaturated fatty acids in the presence of NB. Data presented as mean±s.e.m. (n=3). Significant differences between *cis*- and *trans*-configured unsaturated fatty acids was determined using a paired, two-tailed Student's *t*-test.

Leydig cells (Campos-Silva et al., 2015; O'Shaughnessy et al., 2009) (Fig. 5Cii, white arrow). The dominant population in the SVF was $NR^{+}NB^{+}$ which is consistent with the fluorescence signal shown by the developing spermatozoa in the lumen of the tubules (Fig. 5Di). Flow cytometric analysis of the testes BF showed a complex mixture of cell populations each distinct in their lipid contents (Fig. 5Dii). The majority of cells showed moderate levels of NR and NB, but a subset showed 10-fold higher NB fluorescence (Fig. 5Dii, $NR^{+}NB^{++}$). Additionally, Leydig cells in histological staining showed the highest levels of NR and NB fluorescence (Fig. 5Ci,ii, white arrows).

Muscle cells contain high levels of free fatty acids

Myocytes require fatty acids to fuel contraction (Zlobine et al., 2016). Tile-scan confocal microscopy of sections of entire mouse hearts have demonstrated that the cardiac tissue stained predominantly with NB alone (Fig. 6A). Scattered NR^{+} lipid droplets were detected in the left ventricle and the left and right atrium (Fig. 6Ai). Correspondingly, both the SVF and BF showed predominantly NB staining by flow cytometry (Fig. 6Bi,ii). Together, these data indicate that the cardiac muscle is primarily involved in the metabolism of unsaturated FFA rather than lipid storage. The mouse quadriceps were striking in the variety of NR signals (Fig. 6C). All fibres showed NB fluorescence, similar to cardiac muscle; however, NR signal varied from fibre to fibre (Fig. 6Ci). Muscle fibres that showed higher levels of NB fluorescence also showed NR fluorescence (Fig. 6Ci). This segregation of cell types was evident both in the histological staining and in the flow cytometric profiles of the cells in the SVF (Fig. 6Di). The BF is composed largely of adipocytes. A $NR^{++}NB^{+}$ population is evident in the flow cytometric analysis of the BF (Fig. 6Dii). We attribute this population to the intermuscular adipocytes with the remaining $NR^{+}NB^{+}$ population representing the intramuscular adipocytes (Fig. 6Ci,Dii). Both cardiac and skeletal muscle are dominated by high FFA levels compared to NR-staining lipid droplets.

Multiparametric flow cytometric analyses of the liver using lipid content to distinguish cell types

The adult liver is a site of complex lipid metabolism. Retinol, an autofluorescent form of vitamin A (Vit A) is stored in vacuoles in hepatic stellate cells (HSCs) (Higashi et al., 2005). The autofluorescence signal of retinol is distinct from NR or NB fluorescence and hence can be included in multiparametric analyses. The large data sets generated by multiparametric flow cytometry can be analysed using spanning-tree progression analysis of density-normalised events (SPADE) analyses (Qiu et al., 2011). Vit A-containing cells were located between hepatocytes in close proximity to sinusoidal vessels (Fig. 7A). All HSCs were stained with either NR, NB or both dyes (Fig. 7A). NB and NR staining of the BF of digested liver tissue revealed two populations with different NB

Journal of Cell Science (2022) 135, jcs258322. doi:10.1242/jcs.258322

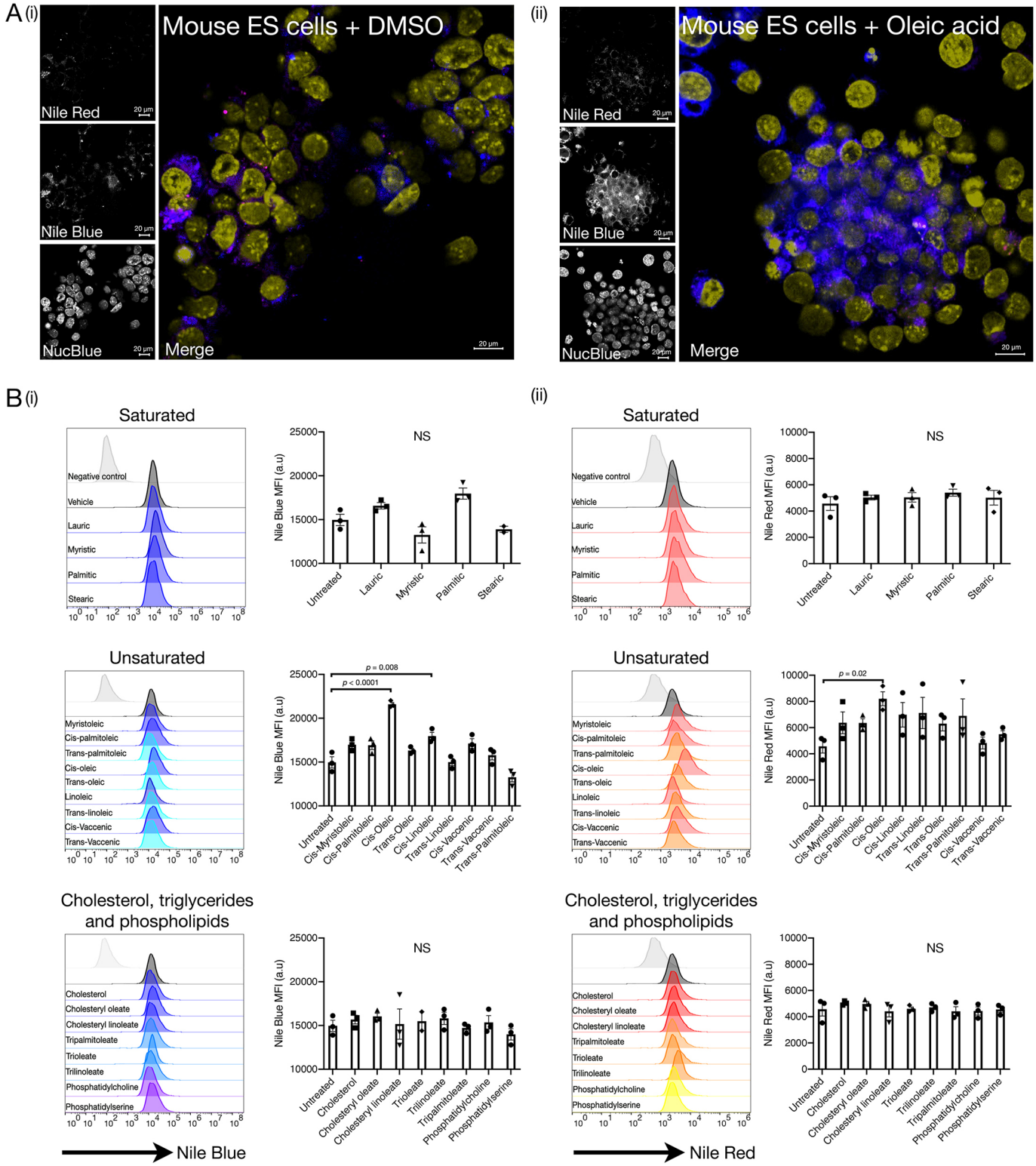

Fig. 3. NB and NR preferentially stain oleic acid in live cells. Representative images of ESCs treated with DMSO (vehicle) (Ai) or oleic acid (Aii) and stained with NR (magenta), NB (blue) and NucBlue (yellow) by confocal microscopy. Images were taken on a single plane. Scale bars: 20 µm. (Bi,ii) Representative flow cytometric histogram plots of NB (Bi) and NR (Bii) mean fluorescence intensity (MFI) in undifferentiated mouse ESCs treated with DMSO (vehicle, light grey) for saturated free fatty acids, unsaturated free fatty acids, cholesterol, cholesterol esters, triglycerides and phospholipids. Data presented as mean±s.e.m. (n=3). Significance in NB and NR fluorescence between lipids was determined by a one-way ANOVA with Tukey's post hoc multiple comparison test (NS, not significant).

Journal of Cell Science (2022) 135, jcs258322. doi:10.1242/jcs.258322

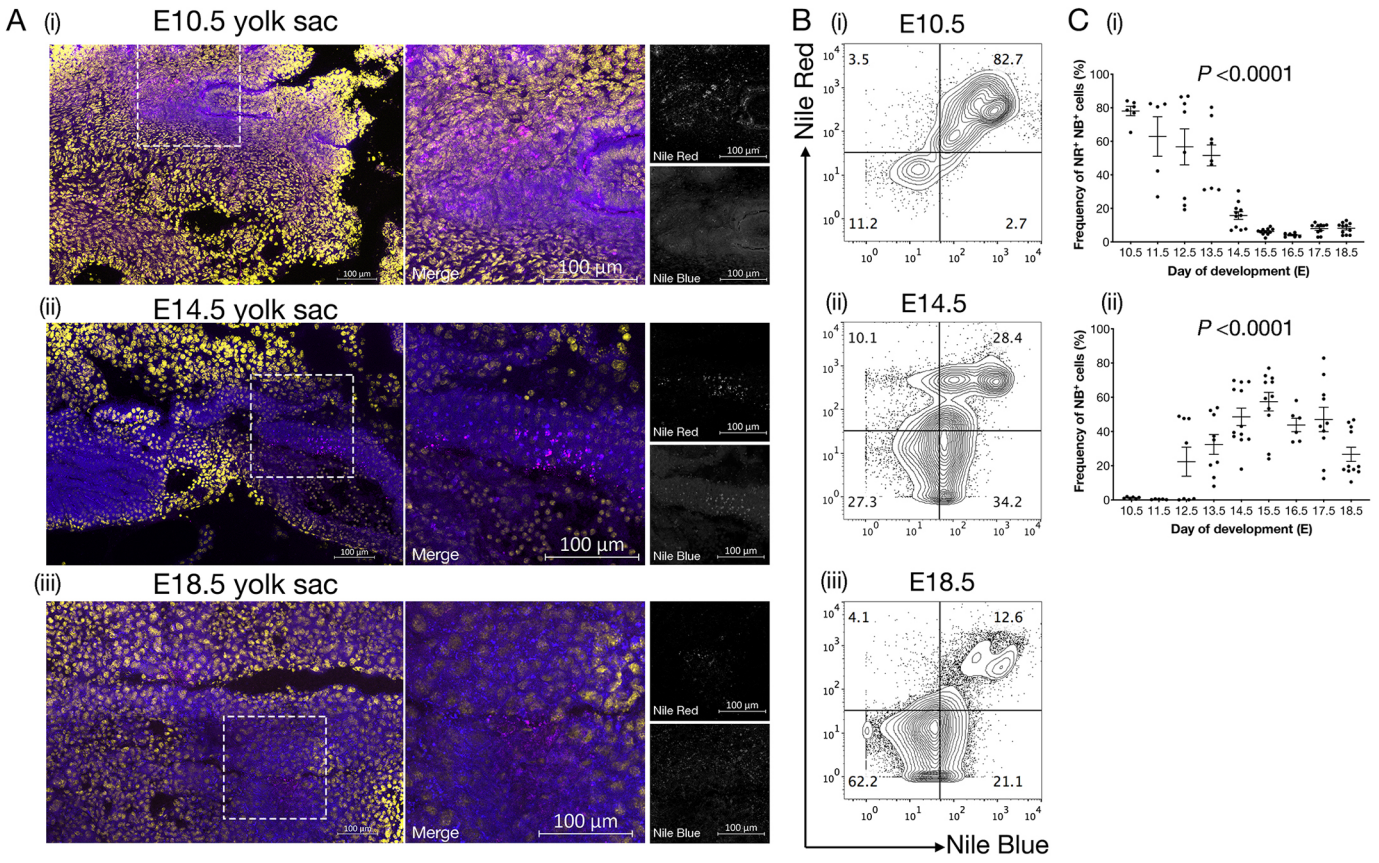

Fig. 4. Co-staining of NB and NR reveals dynamic changes in the metabolism and transportation of lipids. (A) Representative images of 20 µm cryosections of mouse yolk sacs from embryos taken at (i) E10.5, (ii) E14.5 and (iii) E18.5, fixed with 4% PFA, stained with NR (magenta), NB (blue) and DAPI (yellow) by confocal microscopy. A *z*-stack of 20 µm was compiled for each sample. Images presented are a maximum intensity projection. (B) Representative flow cytometric plots of (i) E10.5, (ii) E14.5 and (iii) E18.5 yolk sacs stained with NR and NB. Populations were gated according to NR and NB fluorescence intensity. Numbers inside regions indicate percentage of cells in each area. (C) Comparison of (i) NR and NB double-positive cells (NR^+NB^+) and (ii) NB single-positive cells (NB^+) in the yolk sacs of E10.5–E18.5 embryos (n=10 for each time point). Values presented are means±s.e.m. (n=2–5 independent experiments). Statistical significance was determined using a one-way ANOVA with Tukey post-hoc multiple comparison test. *P*-value indicates overall significance of difference across all groups (pairwise *P*-values are given in Tables S3 and S4).

fluorescence (Fig. 7Bi,ii). Cells with low NB fluorescence (NR^+NB^+) had two populations (19.2% and 3%, respectively) exhibiting Vit A fluorescence (Fig. 7Bi,ii). Conversely, cells with brighter NB staining contained a single population (26%) of Vit A^+ cells (Fig. 7Bi,ii).

To confirm that the data was suitable for exploratory factor analysis, principal component analysis (PCA) on the data-set was performed. The Kaiser–Meyer–Olkin measure of sampling adequacy (0.711) and Bartlett's test for sphericity (approx χ^2=705461; d.f.=36; P<0.001) fell within the acceptable range. NB and Vit A showed highly significant correlations to all other parameters, while NR was significantly correlated to all parameters except for forward scatter (Table S4). There was a particularly strong correlation between Vit A and NR fluorescence but not between Vit A and NB fluorescence. Spectrofluorimetric analysis demonstrated that NR but not NB fluoresced in the presence of retinol when excited (λ_{max} is ∼1200 nm at 488 nm). Retinol alone exhibited fluorescence emission at 405 nm but not 488 nm. The NR signal observed by flow cytometry using the 405 nm excitation laser is therefore most likely indicative of retinol-filled lipid droplets in HSC.

SPADE analyses segregated 16 discrete groups in liver BF cells (Fig. 7Ci,ii; Fig. S2). A breakdown of the putative cell types for each group can be seen in Fig. 7. NR and NB distribution varied across the different groups (Fig. 7Ci,ii). In particular, all groups except 14, 15 and 16 exhibited NB fluorescence while only groups 1, 9, 15 and 16 exhibited NR fluorescence (Fig. 7Ci,ii). The SPADE plot for Vit A autofluorescence revealed two distinct groups with high levels of fluorescence (Fig. 7Ci). Group 16 only contained NR and Vit A fluorescence suggesting differences in HSC maturation stage (Fig. 7Ci,ii). These data demonstrate that multiple lipid classes can be assessed by flow cytometry in live cells using commonly available reagents and autofluorescence signals resolving the complex distribution of lipids in cells, tissues and organs.

DISCUSSION

NB and NR have long been used as histological stains but their utility as probes of specific lipid classes has not been extensively characterised. Here, we demonstrate that NB is a cell-permeable, far-red probe able to detect the presence of unsaturated FFAs with at least 16 carbons, with the *cis* (*Z*-)configuration resulting in higher fluorescence intensity of the dye than the *trans* (*E*-)configuration. In contrast, NR identifies triglycerides, cholesterol and cholesteryl esters but not FFAs. The levels of specificity of both NR and NB allows the identification of biologically important lipids present in mammalian cells when combined. Together with Vit A autofluorescence, we have been able to identify characteristic traits of mammalian cell lipid content using non-destructive, non-toxic and relatively inexpensive reagents in a process we term intracellular

Journal of Cell Science (2022) 135, jcs258322. doi:10.1242/jcs.258322

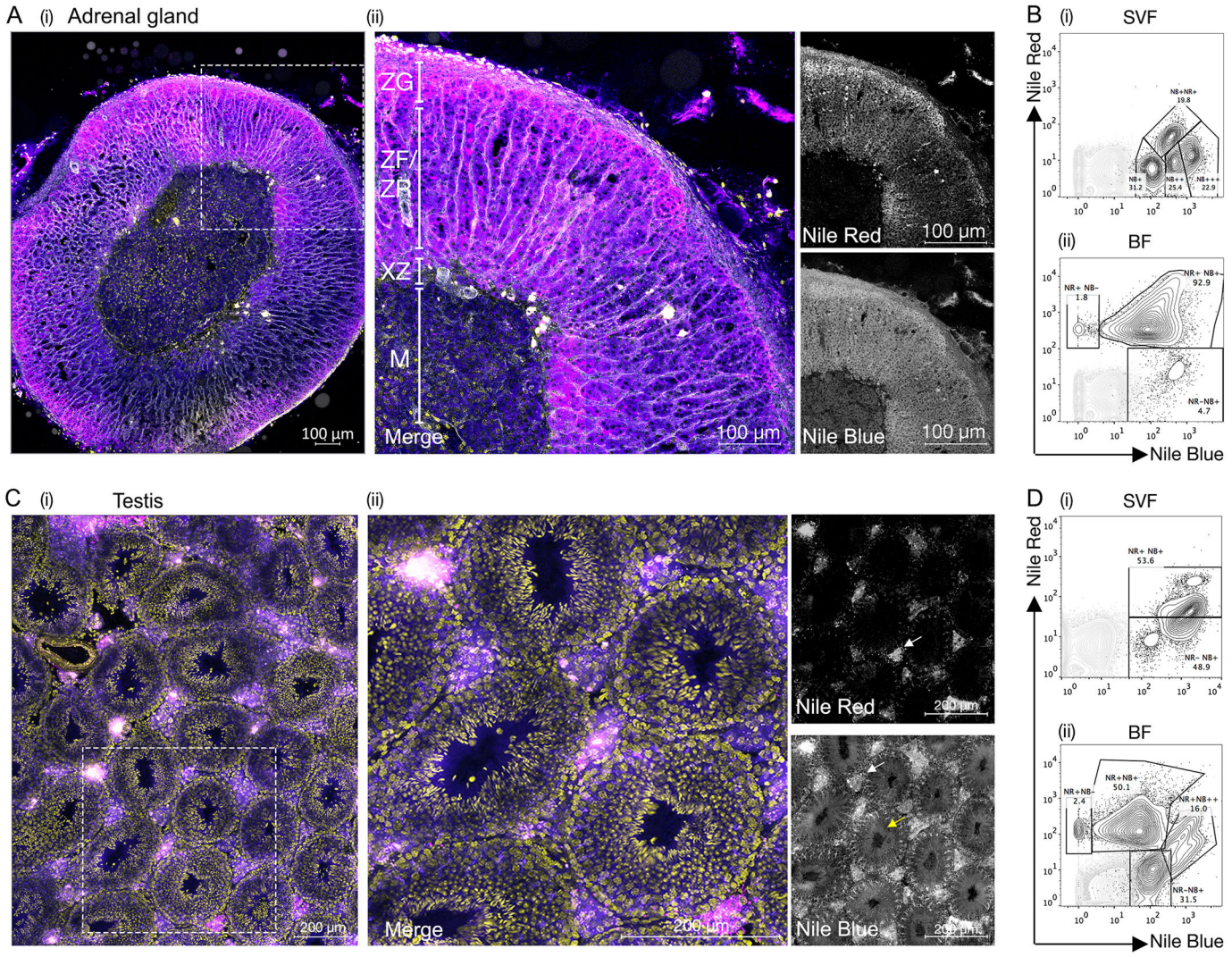

Fig. 5. NB and NR double-staining identifies discrete populations in the mouse adrenal gland and testis. Representative images of 20 µm cryosections of mouse (A) adrenal gland and (C) testis, fixed with 4% PFA, stained with NR (magenta), NB (blue), phalloidin (adrenal only) (grey) and DAPI (yellow) by confocal microscopy. A *z*-stack of 20 µm was compiled for each sample. Magnified regions (white dotted box) of mouse (Aii) adrenal gland and (Cii) testis presented. ZG, zona glomerulosa; ZF, zona fasciculata; ZR, zona reticularis, XZ, z-zone; M, medulla. White arrows in Cii represent Leydig cells. Yellow arrow highlights the seminiferous tubule. Single-cell suspensions of mouse (B) the adrenal gland and (D) testis were generated using the method previously published (Boumelhem et al., 2017). Cells of the stromal vascular fraction (SVF; Ci,Di) and buoyant fraction (BF; Cii,Dii) were stained with NR and NB and fluorescence observed. Gates were applied according to fluorescence intensity: NR positive (NR^{+}), NB positive (NB^{+}), NR high (NR^{++}) or NB high (NB^{++}). For each cell fraction, at least 10^5 cells were collected. Numbers inside regions indicate percentage of cells in each area.

flow cytometric lipid analysis (IFCLA). In the future, IFCLA could be readily adapted to other lipid-sensing probes such as P-IID, a phosphatidylserine-specific sensor (Zwicker et al., 2019).

Changes in cellular lipid content during physiological changes, such as exercise, pregnancy, stress and ageing, can now be more readily assessed at the single-cell level using IFCLA. The FFA demands of cardiac and skeletal myocytes can be monitored by NB fluorescence. Likewise, the lipid contents of hepatic populations could now be more easily investigated. Liver biopsy is commonly used to diagnose non-alcoholic fatty liver disease, the most common cause of abnormal hepatic function among adults (Feldstein et al., 2005). While liver biopsies are invasive, the sample obtained could be analysed for NB, NR and Vit A autofluorescence by flow cytometry to determine lipid content levels at the single-cell level with small amounts of material.

Recently, hyperspectral-stimulated Raman scattering imaging has been combined with mass spectrometric analysis of lipids to reveal that ovarian cancer stem cells possess significantly higher levels of unsaturated lipids compared to the non-cancer stem cell population (Li et al., 2017). Similar studies could now be performed by flow cytometry using lipophilic probes. Populations of interest could be FACS-purified according to lipid content for cell culture, gene, protein or further lipid analysis. Flow cytometric analysis with NB and NR could potentially be used to accelerate the speed of diagnosis of diseases related to lipid dysmetabolism, such as leukodystrophies including Zellweger syndrome, a peroxisome biogenesis disorder (Klouwer et al., 2015), or Niemann–Pick disease where sphingomyelin or cholesterol are not appropriately metabolised (Peake and Vance, 2010). The IFCLA method that we present here, using comparatively inexpensive probes, endogenous autofluorescence and antibody staining, could help develop the field of flow cytometric lipidomics and potentially assist with improving diagnostic systems.

Journal of Cell Science (2022) 135, jcs258322. doi:10.1242/jcs.258322

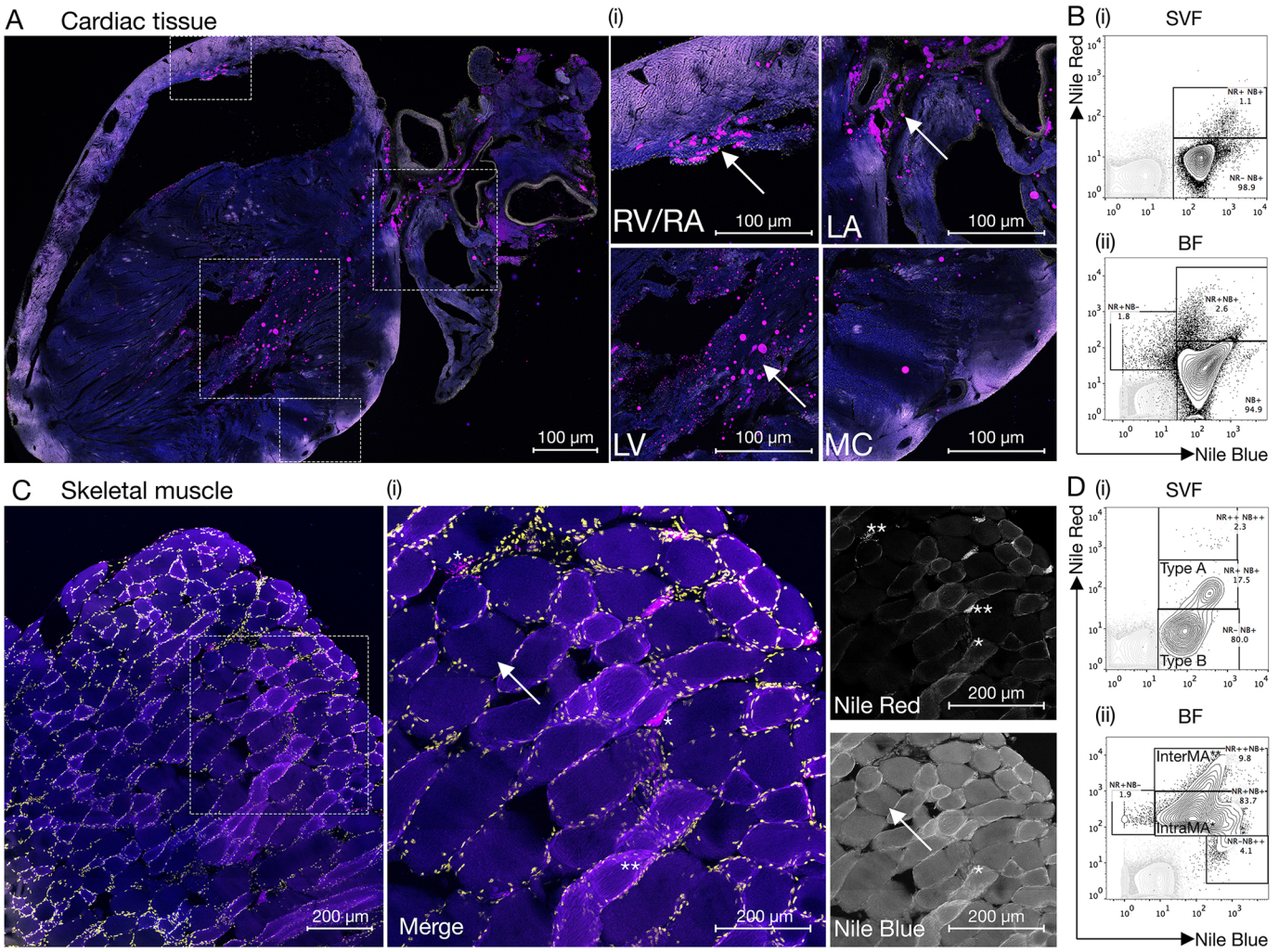

Fig. 6. NB and NR co-staining highlights the distribution of lipids in mouse cardiac and skeletal muscle. Representative images of 20 µm cryosections of mouse (A) heart tissue and (C) skeletal muscle (quadricep) were stained with NR (magenta), NB (blue) and DAPI (yellow) by confocal microscopy. A tile-scan of 1220 images were generated on a single plane for heart tissue. (Ai) Magnified regions (dotted white boxes) of different areas of the mouse heart. RV/RA, right ventricle/atrium; LA, left atrium; LV, left ventricle; MC, myocardium. (Ci) Magnified regions (dotted white box) of skeletal muscle. Arrows indicate different staining patterns of NB in skeletal muscle. Asterisks (* and **) representative of inter- and intramuscular adipocytes, respectively. A *z*-stack of 20 µm was compiled for skeletal muscle and image projected is at maximum intensity. (B,D) Single-cell suspensions of (B) heart tissue and (D) skeletal muscle were generated using the method previously published (Boumelhem et al., 2017). Cells of the stromal vascular fraction (SVF) and buoyant fraction (BF) were stained with NR and NB and fluorescence observed. Two distinct populations (Type A and Type B) were distinguished by lipid contents in skeletal muscle. Gates were applied according to fluorescence intensity: NR positive (NR^+), NB positive (NB^+), NR high (NR^{++}) or NB high (NB^{++}). Putative identity for the most frequent cell type is included. For each cell preparation, at least 10^5 cells were collected. Numbers inside regions indicate percentage of cells in each area.

MATERIALS AND METHODS

Preparation of free fatty acids and lipophilic dyes

FFAs were reconstituted in nitrogen-purged DMSO to a stock concentration of 100 mmol.l^{-1}. NR (N3013, Sigma-Aldrich) was dissolved in DMSO to a stock concentration of 30 mmol.l^{-1}. NB (N0766, Sigma-Aldrich) was dissolved in MilliQ® water to a stock concentration of 10 mmol.l^{-1}.

Spectrofluorometric analyses of NR and NB in the presence of free fatty acids

NR and NB were reconstituted in PBS to a final concentration of 300 nmol.l^{-1} and 1 µmol.l^{-1}, respectively. Lipids were pipetted into a 96-well plate to a final concentration of 100 µmol.l^{-1}. PBS containing NR or NB was then repeatedly pipetted to mix the solution. The plate was inserted into a plate reader (EnSpire, Perkin Elmer) and shaken for 180 s at 60 rpm. NR fluorescence was collected from 510–660 nm (l_ex=488 nm, 5 nm step size) and NB fluorescence was collected from 620–800 nm (l_ex=600 nm, 5 nm step size). Data was collected and exported with EnSpire Workstation software and analysed using Graphpad Prism v7.0.

Cell culture of mouse ESCs

Wild-type, undifferentiated mouse embryonic stem cells (ESCs) (129SV/J, Kuo et al., 2001) were maintained in Dulbecco's modified Eagle's medium (DMEM) supplemented with 10% (v/v) fetal calf serum (FCS), 2 mM Glutamax™, 1 mM sodium pyruvate, 10,000 U.ml^{-1} penicillin, 10 mg.ml^{-1}, streptomycin and 150 µM of 1-thioglycerol. Leukaemia inhibitory factor was added at a concentration of 100 U.ml^{-1} to inhibit spontaneous mouse ESC differentiation. ESCs were validated by assessing Oct3/4 and Nanog gene expression by qRT-PCR. Germ layer potential was assessed routinely to validate the pluripotent nature of the ESC line. Mycoplasma contamination was also assessed routinely and cells have never tested positive.

Confocal imaging of ESCs

Lipid-treated mouse ESCs were washed twice with PBS and then stained with 300 nmol.l^{-1} of NR, 1 µmol.l^{-1} of NB and 0.5 ml of NucBlue (R37605 ThermoFisher Scientific) for 15 min at room temperature. Mouse ESCs were then washed twice with PBS and a cover glass was mounted using

Journal of Cell Science (2022) 135, jcs258322. doi:10.1242/jcs.258322

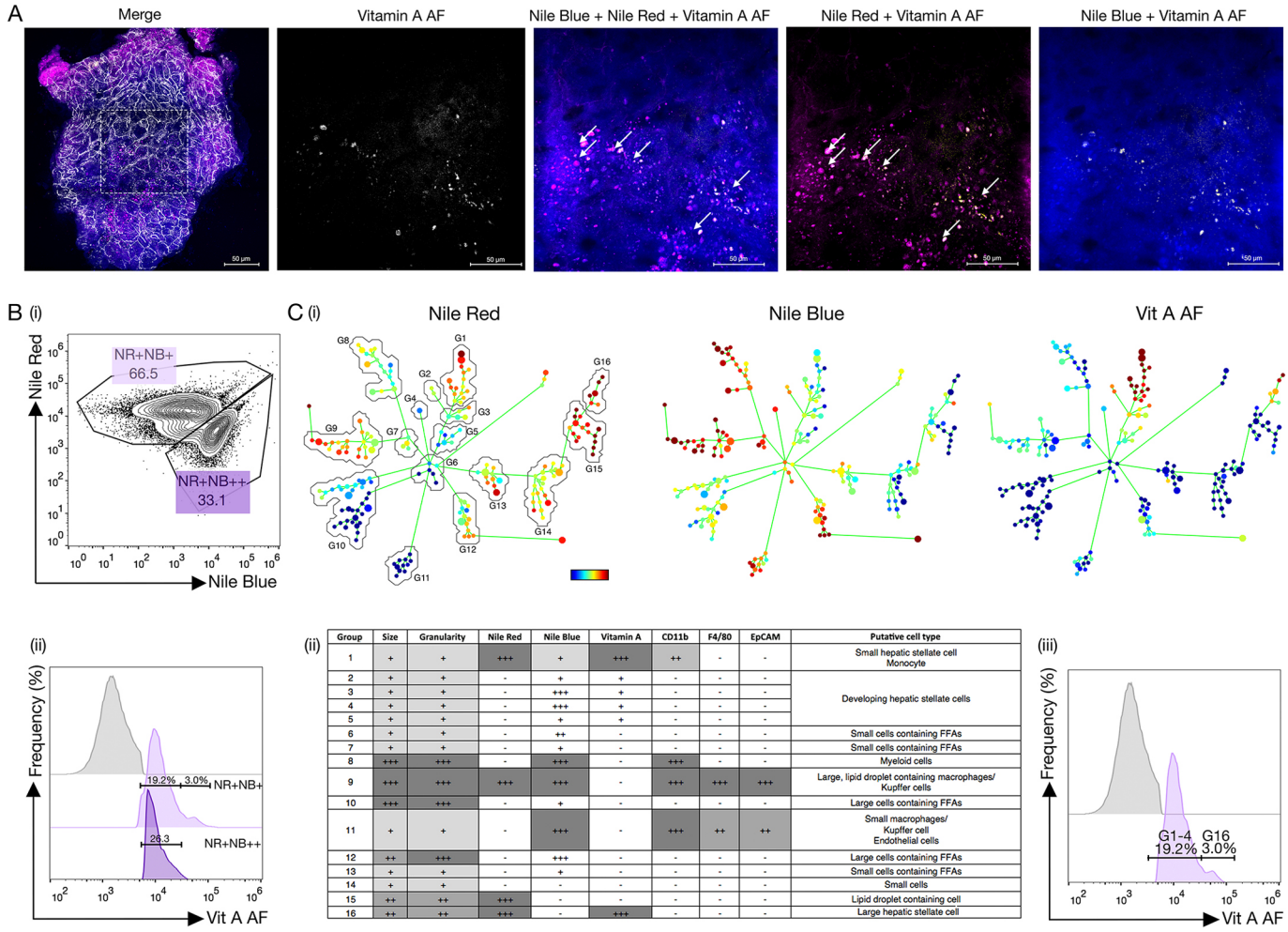

Group	Size	Granularity	Nile Red	Nile Blue	Vitamin A	CD11b	F4/80	EpCAM	Putative cell type
1	+	+	+++	+	+++	++	-	-	Small hepatic stellate cell Monocyte
2	+	+	-	+	+	-	-	-	Developing hepatic stellate cells
3	+	+	-	+++	+	-	-	-	
4	+	+	-	+++	+	-	-	-	
5	+	+	-	+	+	-	-	-	
6	+	+	-	++	-	-	-	-	Small cells containing FFAs
7	+	+	-	+	-	-	-	-	Small cells containing FFAs
8	+++	+++	-	+++	-	+++	-	-	Myeloid cells
9	+++	+++	+++	+++	-	+++	+++	+++	Large, lipid droplet containing macrophages/ Kupffer cells
10	+++	+++	-	+	-	-	-	-	Large cells containing FFAs
11	+	+	-	+++	-	+++	++	++	Small macrophages/ Kupffer cell Endothelial cells
12	++	+++	-	+++	-	-	-	-	Large cells containing FFAs
13	+	+	-	+	-	-	-	-	Small cells containing FFAs
14	+	+	-	-	-	-	-	-	Small cells
15	++	++	+++	-	-	-	-	-	Lipid droplet containing cell
16	++	++	+++	-	+++	-	-	-	Large hepatic stellate cell

Fig. 7. Multiparametric analyses reveals differences in the distribution of lipids in the mouse liver. (A) Representative image of 20 µm cryosection of mouse liver with NR (magenta), NB (blue), vitamin A autofluorescence (yellow) and phalloidin (white) by confocal microscopy. NR and phalloidin were excited at 488 nm; NB was excited at 620 nm and Vitamin A was excited at 408 nm. A *z*-stack of 20 µm was compiled and image projected is at maximum intensity. White arrows represent hepatic stellate cells. (B) Single-cell suspensions of mouse liver were generated using the method previously published (Boumelhem et al., 2017). Cells of the BF were stained with NR and NB and fluorescence observed. Gates were applied according to NR and NB fluorescence intensity and Vitamin A autofluorescence measured in each population. Light purple gated population represents NR-positive, NB-positive cells ($NR^{+}NB^{+}$) while the dark purple gated population represents the NR-positive, NB high cells ($NR^{+}NB^{++}$). Grey histogram peak is representative of the vitamin A-negative population. Numbers inside regions indicate percentage of cells in each area. (Ci) Multiparametric, 'spanning-tree progression analysis of density-normalised events' (SPADE) (Qiu et al., 2011) analyses on the BF of dissociated hepatic tissue. Each node represents a cluster of cells. Blue coloured nodes indicate low levels of fluorescence for that marker while red indicates high levels of fluorescence. Clusters of nodes were grouped together according to differences in fluorescence intensity. Vitamin A autofluorescence was measured in the entire BF of dissociated hepatic tissue and gates applied according to fluorescence intensity. (Cii) Representative groups (G1–16) of the BF according to fluorescence intensity of each parameter and putative cell identity based on fluorescent signals. (Cii) Gated populations in the histogram plot are representative of groups 1–4 and group 16 of the SPADE plot.

VectaShield mounting medium without DAPI (H-1000, Vector Laboratories). The cover glass was sealed using nail polish. Confocal images of lipid-treated mouse ESCs were taken on a Leica SPEII equipped with four solid-state lasers (405 nm, 488 nm, 532 nm and 625 nm). NR was excited using the 488 nm laser and NB was excited using the 625 nm laser. NucBlue was excited using the 405 nm laser. Images were taken on a single plane using an oil-immersed Leica ACS Apochromat 40× objective coupled to the Leica Application Suite – Advanced Fluorescence Software.

Flow cytometry of mouse ESCs

Lipid-treated mouse ESCs were washed twice with PBS followed by addition of 1 ml cell dissociation buffer (Thermo Fisher Scientific). Mouse ESCs were then incubated at 37°C for 10 min. An equal volume of PBS with 0.5% (w/v) BSA (FACS buffer) was added to inactivate the cell dissociation buffer. ESCs were centrifuged for 5 min at 250 ***g***, supernatant was removed and cells re-suspended in 1 ml of FACS buffer. Single-cell suspensions of mouse ESCs were stained with 300 $nmol.l^{-1}$ NR and 1 $\mu mol.l^{-1}$ NB for 15 min. Stained cells were washed with 1 ml of FACS buffer, centrifuged for 5 min at 250 ***g*** and resuspended with FACS buffer containing 0.1% (v/v) propidium iodide and transferred into round bottom FACS tubes. Multi-parametric flow cytometry was performed on a Gallios flow cytometer (Beckman Coulter, Brea, CA, USA) and data collected using the Kaluza G software package. FlowJo V10.1 was used to perform analyses of flow cytometric data.

Mice

Young (8–10 weeks) adult, wild-type, outbred Quackenbush Swiss mice (Animal Resource Centre, Perth, Western Australia) were housed in filter top cages. Mice were kept under a 12-h day–12-h night cycle at constant temperature (21–22°C) and provided food and water *ad libitum*. The welfare of the animals in the housing area and experiments conducted were in accordance with the Australian Code of Practice for the use of animals in research. All animal experimentation work was performed following

approval by the Animal Ethics Committee, University of Sydney. Female mice between 8 and 12 weeks of age were placed with a stud male overnight. The following morning, the females were examined for a vaginal plug. Pregnant females with an observable vaginal plug were classed as 0.5 days pregnant. Pregnant mice were euthanised by cervical dislocation at developmental time points between embryonic day E8.5–E18.5.

Generation of single cell suspensions from primary tissue

Mice were killed by cervical dislocation according to University of Sydney Animal Ethics Committee approval. Dissection and dissociation of brown and white gonadal adipose tissue for flow cytometric was performed as outlined previously (Boumelhem et al., 2017). Brown adipose tissue was dissected from the interscapular region of the mouse while white adipose tissue was excised from the gonadal adipose depot. Skeletal muscle tissue (*biceps femoris*) was dissected from the quadriceps by bilateral incision. Liver, cardiac tissue, the adrenal gland and the testis were also excised for this study. Single-cell suspensions of primary tissues were generated by mincing the tissues into fine pieces (~1–3 mm^3) in FACS buffer containing 0.1% (w/v) collagenase type II (Worthington) for 1 h at 37°C with vigorous shaking every 15 min. Digested tissue was further dispersed with repeated pipetting followed by filtration through a 350 µm polystyrene mesh. An equal volume of FACS buffer was added to the filtered single-cell suspension to inactivate the collagenase and then centrifuged for 5 min at 500 ***g***. Centrifugation pellets were considered as the stromal vascular fraction (SVF) while the buoyant fraction containing adipocytes and lipid-containing cells floats at the surface of the suspension.

Flow cytometric analyses of primary tissue

The buoyant fraction for each tissue was transferred to a separate 15 ml Corning tube while the SVF was resuspended in 1 ml of FACS buffer prior to staining. The SVF and buoyant fraction of each tissue was stained with FACS buffer containing 300 $nmol.l^{-1}$ of NR and 2 $\mu mol.l^{-1}$ of NB for 15 min on ice. For antibody staining of single-cell suspensions, both the buoyant fraction and SVF were stained with the antibodies outlined in Table S5 at a final concentration of 0.5 µg per 1×10^6 cells for 1 h on ice (Table S5). The unbound antibodies were washed with 1 ml of FACS buffer, centrifuged for 5 minutes at 250 ***g*** and supernatant discarded. The cell pellet was resuspended in FACS buffer and transferred to a round bottom tube prior to FACS analysis. Multi-parametric flow cytometry was performed on a Gallios flow cytometer (Beckman Coulter, Brea, CA, USA) and data collected using the Kaluza G software package. FlowJo V10.1 was used to perform analyses of flow cytometric data. Two-tailed correlation analysis of the gated dataset was carried out in SPSS Statistics version 25 (IBM). Dimension reduction was performed using principal component analysis (PCA). Spanning-tree progression analysis of density-normalised events (SPADE) was used to generate and group clusters of cells according to fluorescent antibody and probe staining properties (http://pengqiu.gatech.edu/software/SPADE/27).

Cryosectioning of primary tissues

All tissues assayed were placed in cryomolds (Tissue-Tek, The Netherlands), covered in optimal cutting temperature freezing medium (ProSciTech, Australia), placed in liquid nitrogen to snap freeze and stored at −80°C until needed. Frozen tissues were sectioned with a Leica CM1510S cryostat set at −15°C or −25°C for adipose tissue. All tissues were sectioned at 20 µm before being placed on a Superfrost glass slide (Menzel-Glaser, Germany).

Confocal imaging of NR- and NB-stained tissue

Tissue sections were fixed in 4% (v/v) PFA (in PBS) for 10–20 min at room temperature. Slides were then washed three times in PBS for 5 min each. Slides were stained with 300 $nmol.l^{-1}$ NR and 10 $\mu mol.l^{-1}$ NB in a humidified chamber for 10 min. Slides were then washed twice with PBS for 5 min each and mounted in Vectashield-containing DAPI (Vector Laboratories, USA). High resolution images were taken using a Zeiss LSM 800 confocal microscope coupled with the Zen Blue software package. Nile Red, Nile Blue and DAPI were excited using the 488 nm, 625 nm and 405 nm lasers respectively. To detect and image Vitamin A fluorescence in sections of liver tissue, VectaShield mounting medium without DAPI was used as DAPI is excited at the same wavelength as Vit A (405 nm).

Statistical analyses

All data presented as mean±s.e.m. Statistical analyses were performed using GraphPad Prism®. Comparisons between NR and NB fluorescence in the presence of lipids was determined by a two-tailed paired Student's *t*-test. Differences in NR and NB fluorescence in the yolk sac at different stages of development were determined by one-way ANOVA with a Tukey post-hoc multiple comparison test.

Acknowledgements

We thank the Bosch Institute Live Cell Analysis Facility for assistance with flow cytometry and the Bosch Institute Advanced Microscopy Facility for assistance with confocal microscopy.

Competing interests

The authors declare no competing or financial interests.

Author contributions

Conceptualization: B.B.B., E.J.N., M.L.D., S.J.A., S.T.F.; Methodology: B.B.B., C.P., V.E.Z., J.K., J.H.Y., K.J., E.J.N., M.L.D., S.T.F.; Validation: B.B.B.; Formal analysis: B.B.B., C.P., E.J.N.; Investigation: C.P., V.E.Z., J.K., J.H.Y., S.J.A., S.T.F.; Resources: E.J.N., M.L.D., S.T.F.; Writing - original draft: B.B.B., E.J.N., S.J.A., S.T.F.; Writing - review & editing: B.B.B., K.J., E.J.N., S.J.A., S.T.F.; Visualization: B.B.B., C.P.; Supervision: K.J., S.J.A., S.T.F.; Project administration: B.B.B., S.T.F.; Funding acquisition: S.T.F.

Funding

This work was supported in part by the NWG Macintosh Memorial Award 2019 awarded to B.B.B and S.T.F. J.H.Y. was supported by a Macintosh Scholarship during his PhD studies. This work was also supported in part by a Kickstarter Award from The University of Sydney Nano Institute to S.T.F. and Prof Marcela Bilek (Physics, University of Sydney).

References

Ahlabo, I. and Barnard, T. (1971). Observations of peroxisomes in brown adipose tissue of the rat. *J. Histochem. Cytochem.* **19**, 670-675. doi:10.1177/19.11.670

Astakhova, L., Ngara, M., Babich, O., Prosekov, A., Asyakina, L., Dyshlyuk, L., Midtvedt, T., Zhou, X., Ernberg, I. and Matskova, L. (2016). Short chain fatty acids (SCFA) reprogram gene expression in human malignant epithelial and lymphoid cells. *PLoS One* **11**, e0154102. doi:10.1371/journal.pone.0154102

Boumelhem, B. B., Assinder, S. J., Bell-Anderson, K. S. and Fraser, S. T. (2017). Flow cytometric single cell analysis reveals heterogeneity between adipose depots. *Adipocyte* **6**, 112-123. doi:10.1080/21623945.2017.1319536

Campos-Silva, P., Furriel, A., Costa, W. S., Sampaio, F. J. B. and Gregório, B. M. (2015). Metabolic and testicular effects of the long-term administration of different high-fat diets in adult rats. *Int. Braz. J. Urol.* **41**, 569-575. doi:10.1590/S1677-5538.IBJU.2014.0244

Cespedes, E., Baylin, A. and Campos, H. (2015). Adipose tissue n-3 fatty acids and metabolic syndrome. *Eur. J. Clin. Nutr.* **69**, 114-120. doi:10.1038/ejcn.2014.150

Dates, C. R., Fahmi, T., Pyrek, S. J., Yao-Borengasser, A., Borowa-Mazgaj, B., Bratton, S. M., Kadlubar, S. A., Mackenzie, P. I., Haun, R. S. and Radominska-Pandya, A. (2015). Human UDP-Glucuronosyltransferases: Effects of altered expression in breast and pancreatic cancer cell lines. *Cancer Biol. Ther.* **16**, 714-723. doi:10.1080/15384047.2015.1026480

De la Torre, B., Benagiano, G. and Diczfalusy, E. (1976). Pathways of testosterone synthesis in decapsulated testes of mice. *Acta Endocrinol.* **81**, 170-184. doi:10.1530/acta.0.0810170

Farese, R. V., Cases, S., Ruland, S. L., Kayden, H. J., Wong, J. S., Young, S. G. and Hamilton, R. L. (1996). A novel function for apolipoprotein B: lipoprotein synthesis in the yolk sac is critical for maternal-fetal lipid transport in mice. *J. Lipid Res.* **37**, 347-360. doi:10.1016/S0022-2275(20)37621-5

Feldstein, A. E., Papouchado, B. G., Angulo, P., Sanderson, S., Adams, L. and Gores, G. J. (2005). Hepatic stellate cells and fibrosis progression in patients with nonalcoholic fatty liver disease. *Clin. Gastroenterol. Hepatol.* **3**, 384-389. doi:10.1016/S1542-3565(04)00616-0

Frayn, K. N., Arner, P. and Yki-Järvinen, H. (2006). Fatty acid metabolism in adipose tissue, muscle and liver in health and disease. *Essays Biochem.* **42**, 89-103. doi:10.1042/bse0420089

Greenspan, P., Mayer, E. P. and Fowler, S. D. (1985). Nile red: a selective fluorescent stain for intracellular lipid droplets. *J. Cell Biol.* **100**, 965-973. doi:10.1083/jcb.100.3.965

Griswold, M. D. (1995). Interactions between germ cells and Sertoli cells in the testis. *Biol. Reprod.* **52**, 211-216. doi:10.1095/biolreprod52.2.211

Higashi, N., Sato, M., Kojima, N., Irie, T., Kawamura, K., Mabuchi, A. and Senoo, H. (2005). Vitamin A storage in hepatic stellate cells in the regenerating rat liver: with special reference to zonal heterogeneity. *Anat. Rec. A Discov. Mol. Cell Evol. Biol.* **286**, 899-907. doi:10.1002/ar.a.20230

Hu, J., Zhang, Z., Shen, W.-J. and Azhar, S. (2010). Cellular cholesterol delivery, intracellular processing and utilization for biosynthesis of steroid hormones. *Nutr. Metab. (Lond)* **7**, 47-25. doi:10.1186/1743-7075-7-47

Hu, S., Dong, T. S., Dalal, S. R., Wu, F., Bissonnette, M., Kwon, J. H. and Change, E. B. (2011). The microbe-derived short chain fatty acid butyrate targets miRNA-dependent p21 gene expression in human colon cancer. *PLoS One* **6**, e16221. doi:10.1371/journal.pone.0016221

Kerwin, J. L., Wiens, A. M. and Ericsson, L. H. (1996). Identification of fatty acids by electrospray mass spectrometry and tandem mass spectrometry. *J. Mass Spectrom.* **31**, 184-192. doi:10.1002/(SICI)1096-9888(199602)31:2<184::AID-JMS283>3.0.CO;2-2

Klouwer, F. C., Berendse, K., Ferdinandusse, S., Wanders, R. J., Engelen, M. and Poll-The, B. T. (2015). Zellweger spectrum disorders: clinical overview and management approach. *Orphanet J. Rare Dis.* **10**, 151-111. doi:10.1186/s13023-015-0368-9

Kuo, Y.-M., Zhou, B., Cosco, D. and Gitschier, J. (2001). The copper transporter CTR1 provides an essential function in mammalian embryonic development. *Proc. Natl Acad. Sci. USA* **98**, 6836-6841. doi:10.1073/pnas.111057298

Li, J., Condello, S., Thomes-Pepin, J., Ma, X., Xia, Y., Hurley, T. D., Matei, D. and Cheng, J. X. (2017). Lipid desaturation is a metabolic marker and therapeutic target of ovarian cancer stem cells. *Cell Stem Cell* **20**, 303-314.e5. doi:10.1016/j.stem.2016.11.004

Lodhi, I. J. and Semenkovich, C. F. (2014). Peroxisomes: a nexus for lipid metabolism and cellular signaling. *Cell Metab.* **19**, 380-392. doi:10.1016/j.cmet.2014.01.002

Maekawa, M. and Fairn, G. D. (2014). Molecular probes to visualize the location, organization and dynamics of lipids. *J. Cell Sci.* **127**, 4801-4812.

Martinez, V. and Henary, M. (2016). Nile Red and Nile Blue: applications and syntheses of structural analogues. *Chemistry* **22**, 13764-13782. doi:10.1002/chem.201601570

McMillian, M. K., Grant, E. R., Zhong, Z., Parker, J. B., Li, L., Zivin, R. A., Burczynski, M. E. and Johnson, M. D. (2001). Nile Red binding to HepG2 cells: an improved assay for in vitro studies of hepatosteatosis. *In Vitr. Mol. Toxicol.* **14**, 177-190. doi:10.1089/109793301753407948

Murphy, R. C. and Axelsen, P. H. (2011). Mass spectrometric analysis of long-chain lipids. *Mass Spectrom. Rev.* **30**, 579-599. doi:10.1002/mas.20284

O'Shaughnessy, P. J., Morris, I. D., Huhtaniemi, I., Baker, P. J. and Abel, M. H. (2009). Role of androgen and gonadotrophins in the development and function of the Sertoli cells and Leydig cells: data from mutant and genetically modified mice. *Mol. Cell. Endocrinol.* **306**, 2-8. doi:10.1016/j.mce.2008.11.005

Ostle, A. G. and Holt, J. G. (1982). Nile blue A as a fluorescent stain for poly-beta-hydroxybutyrate. *Appl. Environ. Microbiol.* **44**, 238-241. doi:10.1128/aem.44.1.238-241.1982

Park, H., He, A., Tan, M., Jordan, J. M., Dean, J. M., Pietka, T. A., Chen, Y., Zhang, X., Hsu, F.-F., Razani, B. et al. (2019). Peroxisome-derived lipids regulate adipose thermogenesis by mediating cold-induced mitochondrial fission. *J. Clin. Invest.* **129**, 694-711. doi:10.1172/JCI120606

Peake, K. B. and Vance, J. E. (2010). Defective cholesterol trafficking in Niemann-Pick C-deficient cells. *FEBS Lett.* **584**, 2731-2739. doi:10.1016/j.febslet.2010.04.047

Qiu, P., Simonds, E. F., Bendall, S. C., Gibbs, Jr., K. D., Bruggner, R. V., Linderman, M. D., Sachs, K., Nolan, G. P. and Pievritis, S. K. (2011). Extracting a cellular hierarchy from high-dimensional cytometry data with SPADE. *Nat. Biotechnol.* **29**, 886-891. doi:10.1038/nbt.1991

Rosol, T. J., Yarrington, J. T. and Latendresse, C. C. C. (2001). Adrenal gland: structure, function, and mechanisms of toxicity. *Toxicol. Pathol.* **29**, 41-48. doi:10.1080/019262301301418847

Rui, L. (2011). *Energy Metabolism in the Liver*. John Wiley & Sons, Inc., vol. 97, pp. 177-197.

Rumin, J., Bonnefond, H., Saint-Jean, B., Rouxel, C., Sciandra, A., Bernard, O., Cadoret, J.-P. and Bougaran, G. (2015). The use of fluorescent Nile red and BODIPY for lipid measurement in microalgae. *Biotechnology for Biofuels* **8**, 42. doi:10.1186/s13068-015-0220-4

Smith, J. L. (1911). The staining of fat by Nile-blue sulphate. *Journal of Pathology and Bacteriology* **15**, 53-55. doi:10.1002/path.1700150107

Zlobine, I., Gopal, K. and Ussher, J. R. (2016). Lipotoxicity in obesity and diabetes-related cardiac dysfunction. *Biochim. Biophys. Acta* **1861**, 1555-1568. doi:10.1016/j.bbalip.2016.02.011

Zwicker, V. E., Oliveira, B. L., Yeo, J. H., Fraser, S. T., Bernandes, G. J. L., New, E. J. and Jolliffe, K. A. (2019). A fluorogenic probe for cell surface phosphatidylserine using an intramolecular indicator displacement sensing mechanism. *Angewandte Chemie International Edition* **58**, 3087-3091. doi:10.1002/anie.201812489

Table S1. List of fatty acids assayed in this study. Peak emission (λ_{max}) presented as mean ± SEM (n=3).

Name	Class	C atom #	DB #	ω-pos	Nile Blue λ_{max} 660 nm	Nile Red λ_{max} 575 nm
Cholesterol	Cholesterol	27	1	-	171 ± 4	597 ± 15
Cholesteryl linoleate	Cholesterol ester	45	2	-	281 ± 5	989 ± 22
Cholesteryl oleate	Cholesterol ester	45	3	-	197 ± 8	1230 ± 20
1-oleoyl-2-sn-2-glycerol	Diglyceride	37	0	-	154 ± 10	781 ± 16
Galactoceramide	Phospholipid	40	1	-	130 ± 4	200 ± 14
Glucosylceramide	Phospholipid	46	1	-	603 ± 30	2574 ± 150
L-a-phosphatidyl choline	Phospholipid	42	2	-	437 ± 15	1086 ± 40
Platelet activating factor (PAF)	Phospholipid	26	0	-	451 ± 50	1244 ± 53
Phosphatidyl ethanolamine	Phospholipid	41	2	-	315 ± 14	155 ± 6
Phosphatidyl serine	Phospholipid	42	2	-	480 ± 30	647 ± 26
Phosphatidylinositol (3,4,5)-triphosphate	Phospholipid	47	4	-	130 ± 9	40 ± 2
Sphingomyelin	Phospholipid	47	2	-	160 ± 6	322 ± 22
Myelin basic protein	Protein	-	-	-	134 ± 8	248 ± 5
High density lipoprotein	Protein	-	-	-	1038 ± 44	1289 ± 50
Low density lipoprotein	Protein	-	-	-	661 ± 26	2076 ± 70
Propionic Acid	Saturated	3	0	-	47 ± 3	96 ± 5
Glycerol	Saturated	3	0	-	111 ± 5	120 ± 12
O-phosphorylethanolamine	Saturated	3	0	-	100 ± 5	100 ± 8
Butyric acid	Saturated	4	0	-	282 ± 10	35 ± 2
Hexanoic acid	Saturated	6	0	-	127 ± 8	55 ± 6
D-galactose	Saturated	6	0	-	130 ± 12	135 ± 20
Decanoic acid	Saturated	10	0	-	52 ± 2	119 ± 24
Lauric Acid	Saturated	12	0	-	20 ± 1	10 ± 1
Myristic acid	Saturated	14	0	-	18 ± 2	110 ± 14
Pentadecanoic acid	Saturated	15	0	-	144 ± 6	154 ± 19
Palmitic acid	Saturated	16	0	-	92 ± 4	276 ± 25
Stearic acid	Saturated	17	0	-	107 ± 4	103 ± 10
Heptadecanoic acid	Saturated	17	0	-	361 ± 15	122 ± 10
Nonadecanoic acid	Saturated	19	0	-	37 ± 2	65 ± 4
Arachidic acid	Saturated	20	0	-	414 ± 15	53 ± 4
Heneicosanoic acid	Saturated	21	0	-	91 ± 6	37 ± 5
Lignoceric acid	Saturated	24	0	-	53 ± 4	18 ± 4
Octanoic acid	Saturated	8	0	-	14 ± 1	72 ± 10
Triacetate	Saturated - triglyceride	9	0	-	88 ± 10	120 ± 11
Tributyrate	Saturated - triglyceride	15	0	-	120 ± 15	164 ± 14

Trihexanoate	Saturated - triglyceride	21	0	-	73 ± 9	1186 ± 91
Tridecanoate	Saturated - triglyceride	33	0	-	138 ± 12	3065 ± 180
Tridodecanoate	Saturated - triglyceride	39	0	-	82 ± 8	319 ± 29
Tripalmitate	Saturated - triglyceride	51	0	-	41 ± 3	540 ± 33
Tripalmitoleate	Saturated - triglyceride	51	3	7	203 ± 17	3515 ± 220
Trioleate	Saturated - triglyceride	57	3	9	175 ± 19	2121 ± 159
Trilinoleate	Saturated - triglyceride	57	6	9	70 ± 5	1412 ± 144
Oestrogen	Steroid	18	3	-	66 ± 4	53 ± 3
Estrone	Steroid	18	3	-	31 ± 3	147 ± 6
Dihydrotestosterone	Steroid	19	0	-	161 ± 6	282 ± 10
Testosterone	Steroid	19	0	-	102 ± 4	137 ± 8
Corticosterone	Steroid	21	1	-	154 ± 5	32 ± 2
Deoxycorticosterone	Steroid	21	1	-	120 ± 5	149 ± 9
Progesterone	Steroid	21	1	-	76 ± 2	147 ± 8
Crotonic acid	Unsaturated	4	1	2	111 ± 9	21 ± 1
7-Octenoic acid	Unsaturated	8	1	5	136 ± 5	37 ± 1
2-Decenoic acid	Unsaturated	10	1	5	90 ± 10	50 ± 2
5-Dodecanoic acid	Unsaturated	12	1	7	71 ± 5	117 ± 10
Myristoleic acid	Unsaturated	14	1	5	36 ± 2	37 ± 2
Palmitoleic acid	Unsaturated	16	1	7	1585 ± 41	193 ± 5
Linoleic acid	Unsaturated	18	2	6	1713 ± 67	142 ± 9
Oleic acid	Unsaturated	18	1	9	1867 ± 59	600 ± 30
a-linolenic acid	Unsaturated	18	3	6	244 ± 22	217 ± 15
Cis-vaccenic acid	Unsaturated	18	1	7	1455 ± 35	361 ± 19
Arachadonic acid	Unsaturated	20	4	6	1338 ± 29	348 ± 22
Eicosenoic acid	Unsaturated	20	1	9	1057 ± 49	210 ± 11
Eicosapentanoic acid	Unsaturated	20	5	3	663 ± 25	244 ± 14
1-monooleoyl-rac-glycerol	Unsaturated	21	1	9	130 ± 8	30 ± 2
Erucic acid	Unsaturated	22	1	9	1650 ± 85	335 ± 10
Decosahexanoic acid	Unsaturated	22	6	3	418 ± 45	234 ± 11
Anandamide	Unsaturated	22	4	6	178 ± 24	525 ± 45
Nervonic acid	Unsaturated	24	1	9	894 ± 37	298 ± 29
Palmitelaidic acid	Unsaturated - trans	16	1	7	228 ± 11	109 ± 4
Elaidic acid	Unsaturated - trans	18	1	9	779 ± 38	187 ± 14
Linoelaidic acid	Unsaturated - trans	18	2	6	529 ± 15	62 ± 9
Trans-vaccenic acid	Unsaturated - trans	18	1	7	716 ± 18	303 ± 16
11(E)-Eicosenoic acid	Unsaturated - trans	20	1	9	360 ± 11	91 ± 10
Mineral oil		-	-	-	5 ± 1	1237 ± 122

Table S2. ***Pairwise comparisons of changes in Nile Red fluorescence in the yolk sac across development. P values given, NS = non significant difference.***

Embryonic day (E)	10.5	11.5	12.5	13.5	14.5	15.5	16.5	17.5	18.5
10.5		*NS*	*NS*	*NS*	*<0.0001*	*<0.0001*	*<0.0001*	*<0.0001*	*<0.0001*
11.5			*NS*	*NS*	*<0.0001*	*<0.0001*	*<0.0001*	*<0.0001*	*<0.0001*
12.5				*NS*	*<0.0001*	*<0.0001*	*<0.0001*	*<0.0001*	*<0.0001*
13.5					*<0.0001*	*<0.0001*	*<0.0001*	*<0.0001*	*<0.0001*
14.5						*NS*	*NS*	*NS*	*NS*
15.5							*NS*	*NS*	*NS*
16.5								*NS*	*NS*
17.5									*NS*
18.5									

Table S3. ***Pairwise comparisons of changes in Nile Blue fluorescence in the yolk sac across development. P values given, NS = non significant difference.***

Embryonic day (E)	10.5	11.5	12.5	13.5	14.5	15.5	16.5	17.5	18.5
10.5		*NS*	*NS*	*0.0195*	*<0.0001*	*<0.0001*	*0.0012*	*<0.0001*	*NS*
11.5			*NS*	*0.0261*	*<0.0001*	*<0.0001*	*0.0018*	*<0.0001*	*NS*
12.5				*NS*	*0.0111*	*0.0008*	*NS*	*NS*	*NS*
13.5					*NS*	*0.0357*	*NS*	*NS*	*NS*
14.5						*NS*	*NS*	*NS*	*0.0245*
15.5							*NS*	*NS*	*0.0016*
16.5								*NS*	*NS*
17.5									*NS*
18.5									

Table S4. Principal component analysis correlation matrix for data presented in adult mouse liver SPADE analysis. Significance (1-tailed): * $p<0.05$; ** $p<0.01$

	FSC	SSC	CD11b	NR	PI	EpCAM	NB	F4/80	VitA
Size		*0.546***	*0.247***	*0.061*	*-0.017*	*0.120**	*0.276***	*0.005*	*0.317***
Granularity			*0.356***	*0.635**	*0.287***	*0.240***	*0.641***	*0.137**	*0.844***
CD11b				*0.117**	*-0.422***	*0.232***	*0.520***	*0.204***	*0.560***
NR					*0.501***	*0.349***	*0.501***	*0.301***	*0.747***
PI						*0.202***	*0.231***	*-0.013*	*0.255***
EpCAM							*0.367***	*0.614***	*0.366***
NB								*-0.006*	*0.801***
F4/80									*0.210***
VitA									

Table S5. Fluorescently-conjugated antibodies used for multiparametric flow cytometric analyses in the mouse liver.

Antibody	Fluorophore	Cat #	Clone	Source	Citation
Anti-mouse F4/80	APC	123115	BM8	BioLegend	Schaller, E *et al*. *Mol. Cell. Biol.* 22:8035. (2002)
Anti-mouse CD326 (EpCAM)	PerCP/Cyanine 5.5	118219	G8.8/	BioLegend	Dooley, J *et al*. *J Immunol.* 175:4331. (2005).
Anti-mouse/human CD11b	FITC	101205	M1/70	BioLegend	Iwasaki, A and Kelsall, B. L. 2001. *J. Immunol.* 166:4884 (2001).

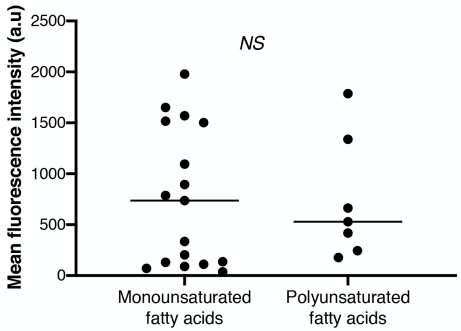

Figure S1: No differences in Nile Blue fluorescence between mono- and polyunsaturated fatty acids.
Spectrofluorimetric analyses of unsaturated fatty acids in the presence of Nile Blue comparing mono- and polyunsaturated fatty acids. Fatty acids were reconstituted in DMSO and pipetted onto a 96-well plate at a final concentration of 100 µmol.L^{-1}. Nile Blue was added to a final concentration of 1 µmol.L^{-1} and excited at 620 nm. Emission was collected from 640 to 800 nm. Data presented as mean ± SEM (n=3). Significant differences between monounsaturated and polyunsaturated fatty acids were determined by Students *t*-test.

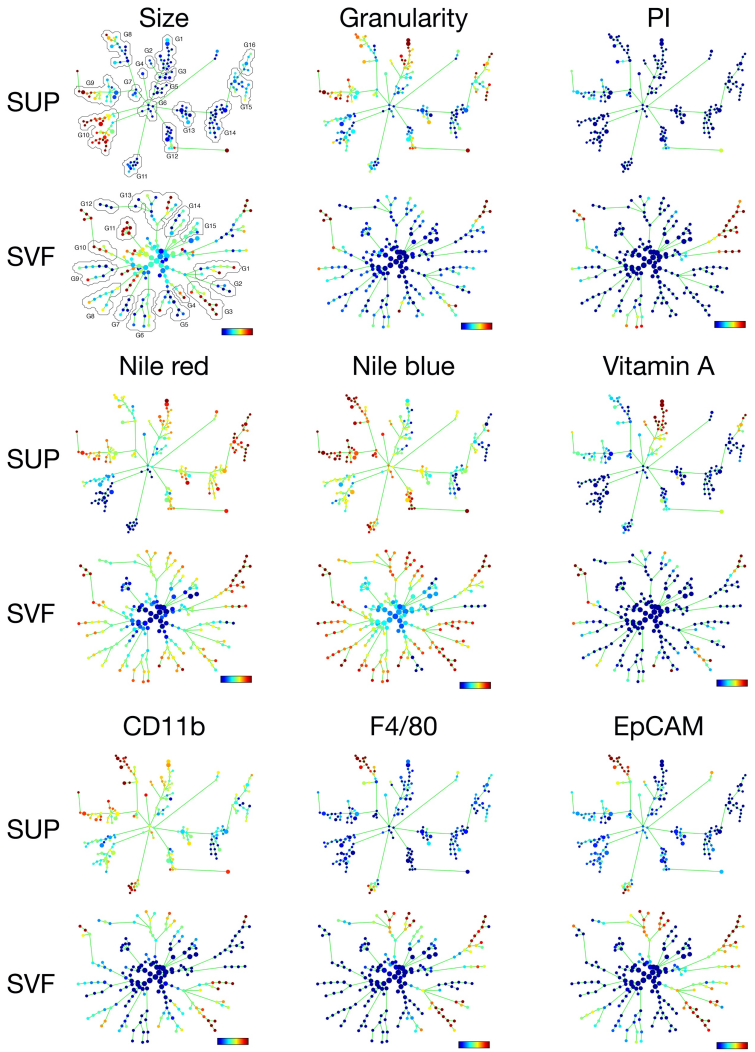

Figure S2: Multiparametric, flow cytometric analyses of hepatic tissue organised by SPADE plots distinguish clusters of lipid rich populations.
Spanning-tree Progression Analysis of Density-Normalised Events' (SPADE)[40] analyses were conducted on the buoyant fraction (BF) and stromal vascular fraction (SVF) of dissociated mouse livers stained with Nile Red, Nile Blue, F4/80, EpCAM, CD11b and propidium iodide. Side scatter (granularity), forward scatter (size) and propidium iodide (PI) were also used to build the SPADE tree consisting of a total of 200 nodes. Each node represents a cluster of cells. Blue coloured nodes indicate low levels of fluorescence for the respective marker while red indicates high levels of fluorescence. Clusters of nodes were grouped together according to differences in fluorescence intensity.

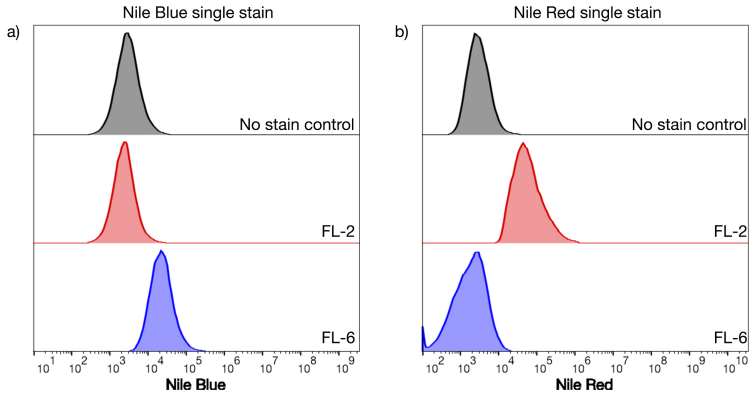

Figure S3: Nile Blue and Nile Red do not overlap in spectral emission by flow cytometry. Single cell suspensions of white adipose tissue were generated using the method previously published[16]. Cells of the buoyant fraction were stained with either Nile Blue (a) or Nile Red (b) and fluorescent populations identified. Fluorescent channel (FL) 6 is excited by the 620 nm laser and detects emission at 660 ± 20 nm. Fluorescent channel (FL) 2 is excited by the 488 nm laser and detects emission at 575 ± 30 nm. Nile Blue (blue shaded plot) and Nile Red (red shaded plot) are only detected in the FL-6 and FL-2 respectively. The black shaded plot represents the no-stain control.

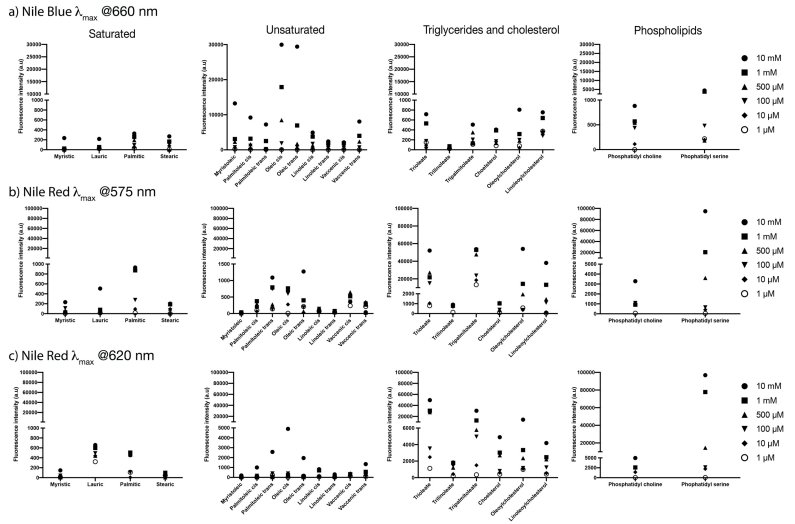

Figure S4: Increasing lipid concentration elicits greater Nile Blue and Nile Red fluorescence.
Spectrofluorimetric analyses of lipids from multiple classes (saturated and unsaturated free fatty acids, cholesterol, cholesterol esters, triglycerides and phospholipids) were performed in the presence of Nile Blue and Nile Red. A dose-response was performed to determine the relationship between lipid concentration and Nile Blue and Nile Red fluorescence. The concentration of lipids ranged from 1 µM - 10 mM. Nile Blue was excited at 620 nm while Nile Red was excited at 488 nm. Peak emission (λ_{max}) for Nile Blue (a) was collected at 660 nm; at 575 nm (b) and 620 nm (c) for Nile Red.